Supporting information

A polymer deposition-mediated surface-charge reformation strategy: Reversing the MOF biomineralization behavior

Yanbin Xu,[a] Huangsheng Yang,[b] Anlian Huang,[b] Linjing Tong,[b] Wei Huang,[c] Guosheng Chen,*[b] Wei Yi,*[a] Siming Huang,*[a] and Gangfeng Ouyang[b,c]

[a] Guangzhou Municipal and Guangdong Provincial Key Laboratory of Molecular Target & Clinical Pharmacology, the NMPA and State Key Laboratory of Respiratory Disease, School of Pharmaceutical Sciences and the Fifth Affiliated Hospital, Guangzhou Medical University, Guangzhou 511436, China
E-mail: yiwei@gzhmu.edu.cn (W. Yi); huangsm@gzhmu.edu.cn (S. Huang)

[b] MOE Key Laboratory of Bioinorganic and Synthetic Chemistry/KLGHEI of Environment and Energy Chemistry, School of Chemistry, Sun Yat-Sen University, Guangzhou 510006, China
E-mail: chengsh39@mail.sysu.edu.cn (G. Chen)

[c] School of Chemical Engineering and Technology, Sun Yat-sen University, 519082 Zhuhai, China.

1. Supplementary Methods

1.1. Reagents and materials.

All chemicals and reagents were purchased from commercial sources and used without further purification. Horseradish peroxidase (HRP, from horseradish, >300 U/mg), bovine serum albumin (BSA), cytochrome c (Cyt c, from Equus caballus heart, >95%), lysozyme (Lys, from chicken egg white, ≥8,000 units/mg), polyacrylic acid (PAA), sodium alginate (SA), β-cyclodextrin (β-CD), γ-cyclodextrin (γ-CD), polyphosphoric acid (PPA), zinc nitrate hexahydrate, rhodamine B (RhB) isothiocyanate, imidazole-2-carboxaldehyde (ICA), glucose, urea, sodium bisulfide (NaHS), luminol, 4-morpholinopyridine (MORP), 3-(10′-phenothiazinyl)-propane-1-sulfonate (SPTZ), ethylene diamine (EDA) and N-(3-dimethylaminopropyl)-N'-ethylcarbodiimide hydrochloride (EDC•HCl) were all purchased from Aladdin Chemistry Co., Ltd. (Shanghai, China). Poly (styrene sulfonic acid) (PSSA) was purchased from Meryer Chemical Technology Co., Ltd. (Shanghai, China). Hyaluronic acid (HA) and α-cyclodextrin (α-CD) were purchased from Macklin Biochemical Technology Co., Ltd. (Shanghai, China). Polyvinyl alcohol (PVA) was purchased from Thermo Fisher Scientific (Shanghai, China). Trypsin (Try, from bovine pancreas, ≥10,000 BAEE units/mg) was purchased from Sigma-Aldrich (Shanghai, China). 2-methyl imidazole (HmIM), zinc acetate dihydrate and 3,3',5,5'-tetramethylbenzidine (TMB) were purchased from J&K Scientific (Beijing, China). Imidazole (IM) was purchased from Fuchen Chemical Reagent Co., Ltd. (Tianjin, China). Hydrogen peroxide (H_2O_2, 30%) was purchased from Guangzhou Chemical Reagent Factory (Guangzhou, China).

1.2. Characterization.

Powder X-ray diffraction (PXRD) patterns were collected (0.02°/step, 0.06 seconds/step) on a Bruker D8 Advance diffractometer (Cu Kα) at room temperature.

The morphology images of the crystals were taken on a SU8010 ultra-high resolution field emission scanning electron microscope (SEM, Hitachi, Japan).

Fourier transform infrared (FT-IR) spectroscopy was performed with a Bruker EQUINOX 55 spectrometer (32 scans in the 4000-400 cm^{-1} spectral range).

Confocal laser scanning microscope (CLSM 880 NLO, Carl Zeiss, Göttingen, Germany) was used to determine the distribution of RhB-labelled enzyme within ZIF-8.

X-ray photoelectron spectroscopy (XPS) analysis was conducted on a Thermo Fisher Scientific K-Alpha system (USA).

Ultraviolet-visible (UV-Vis) absorbance measurements were carried out on a 2800S spectrophotometer (SOPTOP, Shanghai).

Zeta potentials were measured on a Malvern Nano ZS 90 system (USA).

Circular dichroism (CD) spectra were analyzed by a J1700 CD Spectrometer (JASCO, Japan) in the region of 200-250 nm.

Fluorescence spectra were performed on an F97Pro spectrometer (Lengguang Technology, China).

The inductively coupled plasma mass spectrometry (ICP-MS) tests were carried out on an iCAP RQ ICP-MS instrument (Thermo Fisher Scientific, USA).

1.3. Synthesis of standard ZIF-8.

The standard ZIF-8 was prepared in methanol according to the previously reported method.[1] In brief, HmIM (160 mM, 20 mL) and zinc acetate dihydrate (40 mM, 20 mL) were separately dissolved in methanol and then mixed under stirring. After 12 h of reaction, the sediment was collected by centrifugation and washed by methanol 3 times to obtain the standard ZIF-8 crystals.

1.4. Synthesis of the polymers-enzyme@ZIF-8 biominerals.

The preparation of the polymers-enzyme@ZIF-8 biominerals was based on a mild *de novo* approach.[2] In a typical synthetic process, HRP, Cyt c, Lys, or Try (2 mg) was firstly added to the PSSA, PAA, HA, SA, PPA, PVA, α-CD, β-CD, or γ-CD polymer solution. Of specific note, due to the strong acidity of PSSA, the pH of PSSA solution was adjusted to be neutral (~7) in advance by using NaOH solution, meanwhile it is beneficial to expose negatively charged SO_3^- groups. Subsequently, 2.0 mL of HmIM aqueous solution (160 mM) was added to the above polymer-enzyme mixture and then stirred for 30 seconds, followed by an injection of zinc acetate aqueous solution (40 mM, 2.0 mL) into the reaction system. Then, the mixture was stood for 1 h at room

temperature. Finally, the precipitate was collected by centrifugation (10000 rpm, 5 min), and washed with deionized water 3 times.

1.5. Measurement of zeta potential of the polymer-HRP complexes.

0.5 mg of PSSA, PAA, HA, SA, PPA, PVA, α-CD, β-CD, or γ-CD was added to the HRP solution (2 mg, 1mL), followed by 1 h of incubation at room temperature. Afterwards, the unadsorbed polymers were removed by dialysis overnight and then the as-obtained polymer-HRP complex solution was taken for zeta potential measurements.

1.6. Synthesis of aminated BSA (BSA-NH_2).

The BSA-NH_2 was prepared based on a previous work.[3] Briefly, 2 mL of EDA (4.01 mmol, in deionized water) was prepared, and the pH value was adjusted to 4.5 using 1M HCl. Then the BSA (20 mg) was dissolved in the prepared EDA solution, followed by adding 7.2 mg of EDC•HCl (0.038 mmol). The mixture was stirred under 4 °C for 2 h, and subsequently the unreacted agents were removed by dialysis for 24 h.

1.7. Biomineralization of ZIF-8 onto BSA, BSA-NH_2 and PSSA-BSA-NH_2.

In a typical synthetic process, 2 mg of BSA, BSA-NH_2 or PSSA-BSA-NH_2 was firstly added to 2.0 mL of HmIM aqueous solution (160 mM), followed by an injection of zinc acetate aqueous solution (40 mM, 2.0 mL) into the reaction system. Then, the mixture was stood for 1 h at room temperature. Finally, the precipitate generated was collected by centrifugation (10000 rpm, 5 min), and washed with deionized water 3 times.

1.8. Surface acetylation modification of HRP via chemical coupling.

The surface acetylation modification of HRP via a chemical coupling method was achieved according to a previous report.[3] 10 mg HRP was firstly dispersed in 4 mL phosphate buffered saline (PBS, 100 mM, pH=8). Then a 100-fold molar acetic anhydride solution (in 2 mL deionized water) was added drop-by-drop under stirring. The pH of the solution was adjusted back to 8 using 0.5 M NaOH and followed by stirring for 60 min. At last, the acetylated HRP was obtained through dialysis for 12 h to remove excess reaction reagents and salts and then freeze-dried for further use.

1.9. Measurement of loading contents of enzymes.

The loading contents of enzymes within MOFs were measured by examining the concentration distinctions of enzymes in the supernatants before and after synthesis via using a standard BCA assay. Typically, 20 μL of enzyme sample was added into a 96-well plate, followed by introducing 200 μL of BCA working solution. After incubating at 60 °C for 15 min, the solution was collected and detected by a UV-Vis spectrophotometer. The concentration of the enzyme was proportional to the absorbance at 562 nm.

1.10. CLSM experiment for polymers-HRP@ZIF-8.

HRP enzymes were first labelled by the RhB isothiocyanate dye (denoted as RhB-HRP). In detail, 1 mg RhB isothiocyanate and 20 mg HRP were dissolved into 10 mL PBS buffer (pH=9.0) and subsequently stirred for 4 h. And then, the mixture was dialyzed to remove the unreacted dyes, followed by freeze-drying to obtain RhB-HRP solids. Afterwards, the RhB-HRP was used to prepare the polymers-HRP@ZIF-8 as described above and the as-synthesized polymers-RhB-HRP@ZIF-8 biominerals were used for CLSM experiments.

1.11. Examination of bioactivity of polymers-HRP@ZIF-8 composites.

The bioactivities of HRP and polymers-HRP@ZIF-8 were evaluated through tracing the decomposition of H_2O_2 using TMB as a chromogenic reagent based on Equation 1: [4]

$$H_2O_2 + TMB \overset{HRP}{\rightarrow} H_2O + oxTMB \quad (1)$$

The concentration of the used polymers-HRP@ZIF-8 in examinations were controlled to be 2 μg/mL according to the calculated loading content, unless otherwise stated. In a typical test, 100 μL of the polymer-HRP@ZIF-8 solution was added to the cuvette, followed by adding 100 μL of TMB solution (100 μg/mL). Immediately, 200 μL H_2O_2 (0.1 mM) was added to activate the catalytic reaction and then oxidize the TMB to be oxTMB which could be traced at 652 nm by UV-Vis spectrophotometer using a time-scanning mode.

1.12. Measurement of the kinetic parameters of polymers-HRP@ZIF-8.

The catalytic kinetic parameters were measured according to the Michaelis-Menten equation (Equation 2):[5]

$$V_o = \frac{V_{max}[S]}{K_m + [S]} \quad (2)$$

Here, V_0 is the initial catalytic rate. V_{max} is the maximum rate conversion, which is obtained when the catalytic sites on the enzyme are saturated with substrate. [S] is the initial substrate concentration, and K_m is the Michaelis Menten constant. The initial catalytic rates V_0 was determined by making the slope of the kinetic curve in the initial phase (t from 0 to 20 s), and the initial substrate concentration [S] was determined at t=0 s. The kinetic parameters K_m and V_{max} were fitted using a Michaelis–Menten equation based on the calculated V_0 and [S]. The analysis was performed with the GraphPad prism software (version 9.0.0, GraphPad Software, Inc., San Diego, CA).

1.13. Simulation calculations.

The polymer molecular fragment models were built in Gaussview 6.0 and the density functional theory (DFT) calculations were carried out using Gaussian 09 program. Geometry optimization and frequency analysis were calculated at PBE0 hybrid functional under the level of 6-311G* basis sets and implicit solvation model. The electrostatic potential (ESP) surfaces were calculated at B3LYP hybrid functional with GD3BJ correction under the level of 6-311+G* basis sets and implicit solvation model, and analyzed by Multiwfn 3.8[6] and VMD v 1.9.3 molecular visualization software[7].

1.14. Biomineralization of ZIF-90 onto BSA, BSA-NH_2 and PSSA-BSA-NH_2.

Typically, 2 mg of BSA, BSA-NH_2 or PSSA-BSA-NH_2 was firstly mixed with 2.0 mL of ICA aqueous solution (160 mM), followed by an injection of zinc acetate aqueous solution (40 mM, 2.0 mL) into the reaction system. Then, the mixture was stood for 1 h at room temperature. Finally, the precipitate generated was collected by centrifugation (10000 rpm, 5 min), and then washed with deionized water 3 times.

1.15. Biomineralization of ZIF-zni onto BSA, BSA-NH_2 and PSSA-BSA-NH_2.

First, 2 mg of BSA, BSA-NH_2 or PSSA-BSA-NH_2 was mixed with 2.0 mL IM aqueous solution (160 mM). Then zinc acetate aqueous solution (40 mM, 2.0 mL) was

injected into the reaction system. Then, the mixture was stirred for 1 h at room temperature. Finally, the precipitate was collected by centrifugation (10000 rpm, 5 min), and then washed with deionized water 3 times.

1.16. Synthesis of PSSA-HRP@ZIF-90.

To prepare PSSA-HRP@ZIF-90, HRP (2 mg) was firstly mixed with PSSA (0.5 mg), and subsequently, 2.0 mL of ICA aqueous solution (160 mM) was added to the above polymer-enzyme mixture and then stirred for 30 s, followed by an injection of zinc nitrate aqueous solution (40 mM, 2.0 mL) into the reaction system. Then, the mixture was stood for 1 h at room temperature. Finally, the precipitate was collected by centrifugation (10000 rpm, 5 min), and then washed with deionized water 3 times.

1.17. Synthesis of PSSA-HRP@ZIF-zni.

The PSSA-HRP@ZIF-zni was prepared by mixing HRP (2 mg) with PSSA (0.5 mg) in advance, followed by adding 2.0 mL IM aqueous solution (160 mM) and stirring for 30 s. Then zinc acetate aqueous solution (40 mM, 2.0 mL) was injected into the reaction system. Then, the mixture was stirred for 1 h at room temperature. Finally, the precipitate was collected by centrifugation (10000 rpm, 5 min), and then washed with deionized water 3 times.

1.18. ICP-MS detection of Zn amount.

First, for detecting the Zn amount onto the bare enzyme, 2 mg HRP was added to 4 mL zinc acetate (40 mg) solution and incubated for 1 h at room temperature. After that, the unabsorbed Zn^{2+} was completely excluded via ultrafiltration and the resultant HRP-Zn^{2+} complex was freeze-dried for further ICP-MS analysis. Likewise, for detecting the Zn amount onto the PSSA-HRP complex, 2 mg HRP was first incubated with 0.5 mg PSSA to obtain PSSA-HRP as described previously, and then the PSSA-HRP solid was added to 4 mL zinc acetate (40 mg) for 1 h of incubation to fully interact with Zn^{2+}. Similarly, the mixture was ultrafiltered to remove the free Zn^{2+} to obtain PSSA-HRP-Zn^{2+} complex for ICP-MS analysis.

1.19. Optimization of sensing conditions.

To realize the best analytical performance of the biosensor, experimental conditions including the luminol and H_2O_2 concentrations were optimized. In addition, a

combination of MORP and SPTZ was employed as a dual-enhancer system to simultaneously amplify the luminescence intensity and increase the luminescence time of luminol according to a previous study.[8] Briefly, the PSSA-HRP@ZIF-8 was dispersed into deionized water to set up an HRP concentration of 1 μg/mL. To gain the optimal luminol concentration, 30 μL PSSA-HRP@ZIF-8 solution was added to the opaque 96-well plates with 50 μL PBS buffer, followed by adding 100 μL luminol with different concentrations as well as 30 μL MORP (18 mM) and 30 μL SPTZ (3 mM). And then, 60 μL H_2O_2 aqueous solutions (10 mM) were introduced to the plates and the microplate reader started to record the time-dependent curves immediately.

After the optimization of the luminol concentration, luminol with a final concentration of 1.5 mM was chosen for the further optimization of H_2O_2 concentration. In practice, the operation steps were the same to luminol optimization. Briefly, 30 μL of the prepared PSSA-HRP@ZIF-8 solution was added to the opaque 96-well plates with 50 μL PBS buffer followed by adding 100 μL luminol with a final concentration of 1.5 mM. Then 30 μL MORP (18 mM) and 30 μL SPTZ (3 mM) were added, respectively, and 60 μL H_2O_2 aqueous solution with different concentrations were introduced to the plates, and the microplate reader started to record the time-dependent curves immediately. It is noted that the HRP concentration in the above reaction systems was 0.1 μg/mL.

1.20. H_2S biosensing.

30 μL of the PSSA-HRP@ZIF-8 solution was added in prior to the opaque 96-well plates with 20 μL PBS buffer and then 30 μL NaHS aqueous solution was introduced, followed by adding 100 μL luminol with optimized concentration as well as 30 μL MORP (18 mM) and 30 μL SPTZ (3 mM). At last, 60 μL H_2O_2 aqueous solution was added, and the microplate reader worked immediately. It is noted that the HRP concentration in the reaction system was 0.1 μg/mL.

1.21. Recycle experiment.

To avoid signal decrease caused by the biomineral loss, a higher concentration of biocatalyst was used, where PSSA-HRP@ZIF-8 was dispersed into deionized water to set up an HRP concentration of 1 mg/mL. In the recycle experiments, 30 μL NaHS

aqueous solution (10 mM) and 60 μL H_2O_2 aqueous solutions (10 mM) were in prior introduced into the opaque 96-well plates and mixed for 2 min. And then 20 μL deionized water, 100 μL luminol (4.5 mM), 30 μL MORP (18 mM) as well as 30 μL SPTZ (3 mM) were added, respectively. As last, 30 μL of the as-prepared PSSA-HRP@ZIF-8 was added into the mixture and the microplate reader started to record the time-dependent curves immediately. It is noted that the final HRP and H_2S concentrations in the reaction system were 0.1 mg/mL and 1 mM, respectively. After 1 min record of the signals, the mixture was taken into the centrifuge tube and centrifuged to remove the supernatant. The remained sediment was re-dispersed into 30 μL deionized water and taken for the next detection cycle.

2. Supplementary Tables

Table S1. Information of the polymers selected for the enzyme modification.

Polymers	Functional groups	Molecular weight (Da)	Zeta potential (mV)
PSSA	$-SO_3H$	45000-70000	-25.47±1.94
PAA	-COOH	2000	-7.52±2.16
HA	-COOH, -OH, -CONH	30000-45000	-14.77±3.26
SA	-COOH, -OH	<2000	-44.83±4.54
PPA	$-PO_4^{3-}$	/	-8.77±0.33
PVA	-OH	20000-30000	-3.71±0.59
α-CD	-OH	972.84	-4.78±1.66
β-CD	-OH	1134.98	-3.66±0.21
γ-CD	-OH	1297.12	-6.93±0.77

Table S2. The loading contents of HRP in different polymers-HRP@ZIF-8 biohybrids.

Polymers	Polymer dosage (mg)	Loading amount (%, w/w)
PSSA	0.5	14.02
	1.0	6.90
	4.0	3.21
PAA	0.5	8.75
	1.0	6.84
	4.0	4.20
HA	0.5	4.69
	1.0	3.74
	4.0	2.49
SA	0.5	9.36
	1.0	8.89
	4.0	7.29

Table S3. The loading contents of HRP within MOF reported by previous works.

Enzyme@MOF	Encapsulation strategy	Loading content (%, w/w)	Ref.
HRP@ZIF-8	Biomineralization promoted by polyvinylpyrrolidone/cysteine	14.4	[1]
HRP-A@ZIF-8	Biomineralization promoted by acetic anhydride modified HRP	0.9	[3]
HRP@ZIF-8	Biomineralization promoted by γ-poly-L-glutamic acid	0.24-0.59	[9]
PCN-333/ChOx&HRP	Infiltration	8.0	[10]
HRP@HZIF-8[a]	Infiltration	14.1	[11]
GOx&HRP/ZIF-8	Co-precipitation	6.0	[12]
HRP-MOF[b]	Co-precipitation	4.71	[13]
PSSA-HRP@ZIF-8	Biomineralization	14.02	This work

[a] HZIF-8 represents that the ZIF-8 possessed hierarchical micro- and mesoporous structures which was synthesized by a hydrogel template method.
[b] The MOF is ZIF-8 synthesized by a microfluidic flow synthesis method.

Table S4. The loading contents of other enzymes embedded within ZIF-8.

Sample	Loading efficiency (%)	Loading amount (%, w/w)
PSSA-Cyt c@ZIF-8	91.87	15.31
PSSA-Lys@ZIF-8	35.06	9.61
PSSA-Try@ZIF-8	93.57	14.07
PAA-Cyt c@ZIF-8	74.07	14.24
PAA-Lys@ZIF-8	35.17	6.34
PAA-Try@ZIF-8	95.29	13.33
HA-Cyt c@ZIF-8	46.32	9.36
HA-Lys@ZIF-8	4.86	0.92
HA-Try@ZIF-8	94.69	16.19
SA-Cyt c@ZIF-8	74.06	14.11
SA-Lys@ZIF-8	35.30	7.13
SA-Try@ZIF-8	97.09	17.49

Table S5. The loading contents of HRP confined within ZIF-90 and ZIF-zni induced from PSSA.

Sample	Loading efficiency (%)	Loading amount (%, w/w)
PSSA-HRP@ZIF-90-0.5 mg[a]	15.81	5.55
PSSA-HRP@ZIF-90-1.0 mg[b]	25.66	8.41
PSSA-HRP@ZIF-zni-0.5 mg[a]	54.82	12.75
PSSA-HRP@ZIF-zni-1.0 mg[b]	55.30	12.29

[a] 0.5 mg in the name represents the dosage of PSSA is 0.5 mg.
[b] 1.0 mg in the name represents the dosage of PSSA is 1.0 mg.

Table S6. The Zn and P contents of each digested sample.

	Zn content (μg)	P content (μg)
Pristine PSSA-HRP@ZIF-8 biocomposite	84.69 ± 11.41	0 ± 0.78
Pristine 10 mM PBS solution[a]	0 ± 0.30	5.80 ± 0.17
PSSA-HRP@ZIF-8 biocomposite after exposure to 10 mM PBS solution[b]	89.97 ± 11.50	3.03 ± 0.12
Supernatant of PSSA-HRP@ZIF-8 biocomposite after exposure to 10 mM PBS solution	0.06 ± 0.05	2.15 ± 0.14

[a] The volume of 10 mM PBS (pH 7.4) for the test was 20 μL.
[b] 30 μL PSSA-HRP@ZIF-8 biocomposite with HRP of 100 μg/mL was treated by 20 μL 10 mM PBS (pH=7.4) for 1 min.

Table S7. Comparison of the analytical performance with previously reported biosensors for H_2S detection.

Biosensor	Method	Linear range	LOD	Ref.
AD-3	Fluorescence	0-100 μM	0.19 μM	[14]
Au@MPBN@ Au@4-NTP	Surface-enhanced Raman scattering (SERS)	0.25-20 μM	0.24 μM	[15]
MOF-818	Colorimetry	0.066-100 μM, 100-400 μM	3.5 μM	[16]
MOF-818	Electrochemistry	0.001-0.5 μM, 0.5-2000 μM	0.76 nM	[16]
$F1^{2+}$-ANP	Luminescence	0-50 μM	0.1 μM	[17]
BDP-H_2S	Photoacoustic imaging	0-100 μM	0.59 μM	[18]
AM-BODIPY-NBD	Fluorescence	5-50 μM	15.7 nM	[19]
$CsCu_2I_3$/MOF-801	Photoelectrochemistry	0.005-100 μM	1.67 nM	[20]
BFPP	Fluorescence	0.05-4.0 μM	17 nM	[21]
AuNWs/CNTs/ PDMS	Electrochemistry	5 nM-24.9 μM	3 nM	[22]
Mindo-SiR	Fluorescence	0-20 μM	0.45 μM	[23]
Cy796	Fluorescence	0-12μM, 16-56 μM	27.0 nM	[24]
DSP	Colorimetry	0.5-40 μM	2.17 μM	[25]

DSP	Fluorescence	0.5-20 μM	2.5 μM	[25]
ZAB-SPES	Electrochemistry	5-1000 μM	4 μM	[26]
DCP-H_2S	Fluorescence	1.0-40.0 μM	0.25 μM	[27]
Bcy-HS	Fluorescence	0-100 μM	1.3 μM	[28]
PSSA-HRP@ZIF-8	Chemiluminescence	4.88-78.13 nM	0.09 nM	This work

AD-3: A single-molecule two-photon fluorescent probe;

MPBN: 4-mercaptobenzonitrile;

4-NTP: 4-nitrothiophenol;

$F1^{2+}$-ANP: A H_2S-activatable NIR afterglow probe;

BDP-H_2S: A H_2S-activated ratiometric photoacoustic (PA) probe;

AM-BODIPY-NBD: An NBD-based cell-trappable probe;

$CsCu_2I_3$: A lead-free perovskite cesium copper iodide;

BFPP: A nanobeacon;

AuNWs/CNTs/PDMS: A sensor based on gold nanowire (AuNW) and carbon nanotube (CNT) films embedded in poly(dimethylsiloxane) (PDMS);

SiR: Near-infrared fluorescent probes based on a hemicyanine and Si-rhodamine structure;

Cy796: A H_2S-responsive fluorescence probe;

DSP: A colorimetric and fluorescent dual-mode sensing platform;

ZAB: Zinc-air battery;

SPES: Self-powered electrochemical sensor;

DCP-H_2S: A near-infrared fluorescent probe based on isophorone-xanthene dye for sensing hydrogen sulfide (H_2S);

Bcy-HS: A fluorescent probe.

3. Supplementary Figures

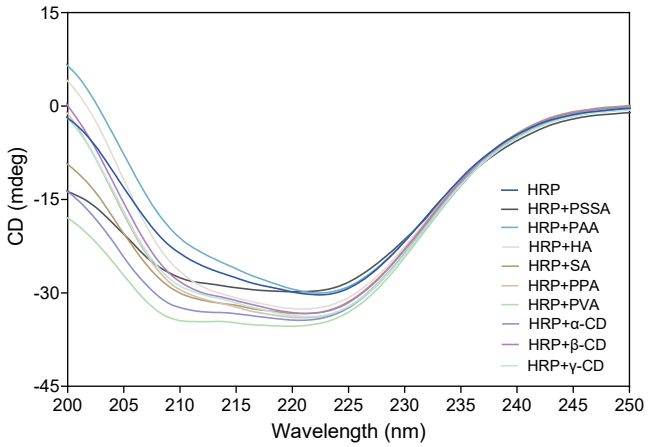

Fig. S1. CD spectra of free HRP, and the mixed solutions consisting of HRP and the polymers, respectively.

Note: 2 mg of HRP was first incubated with 0.5 mg of individual polymer, and then the concentration of HRP was diluted to 0.25 mg/mL in each test.

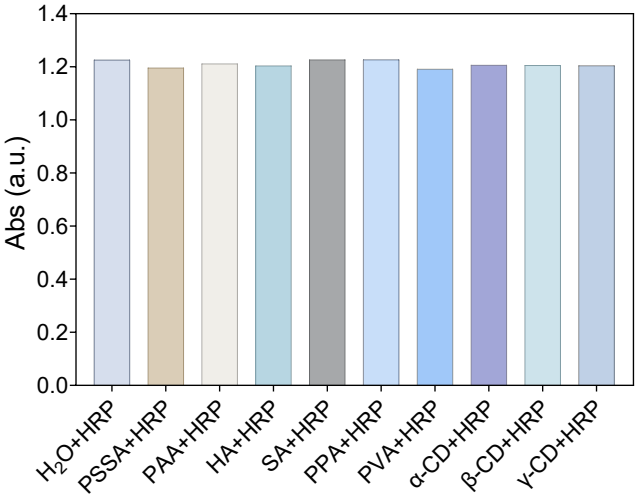

Fig. S2. The catalytic activities of free HRP and polymers-HRP complexes assessed by UV-vis.

Note: 2 mg of HRP was pre-treated by 0.5 mg of the polymer for 1 h, and then the catalytic activities of the polymers-HRP composite were tested by tracing the generation of oxTMB at 652 nm. The results showed that all the polymers-HRP complexes showed comparable activity to the free HRP.

Fig. S3. The photographs recording the growth phenomenon of ZIF-8 minerals in the presence of PSSA, PAA, HA and SA, respectively. The amount of each polymer used for synthesis is 0.5 mg.

Note: The phenomena suggested the capability of these polymers as biomimetic mineralization agents to form PSSA@ZIF-8, PAA@ZIF-8, HA@ZIF-8, and SA@ZIF-8 composites.

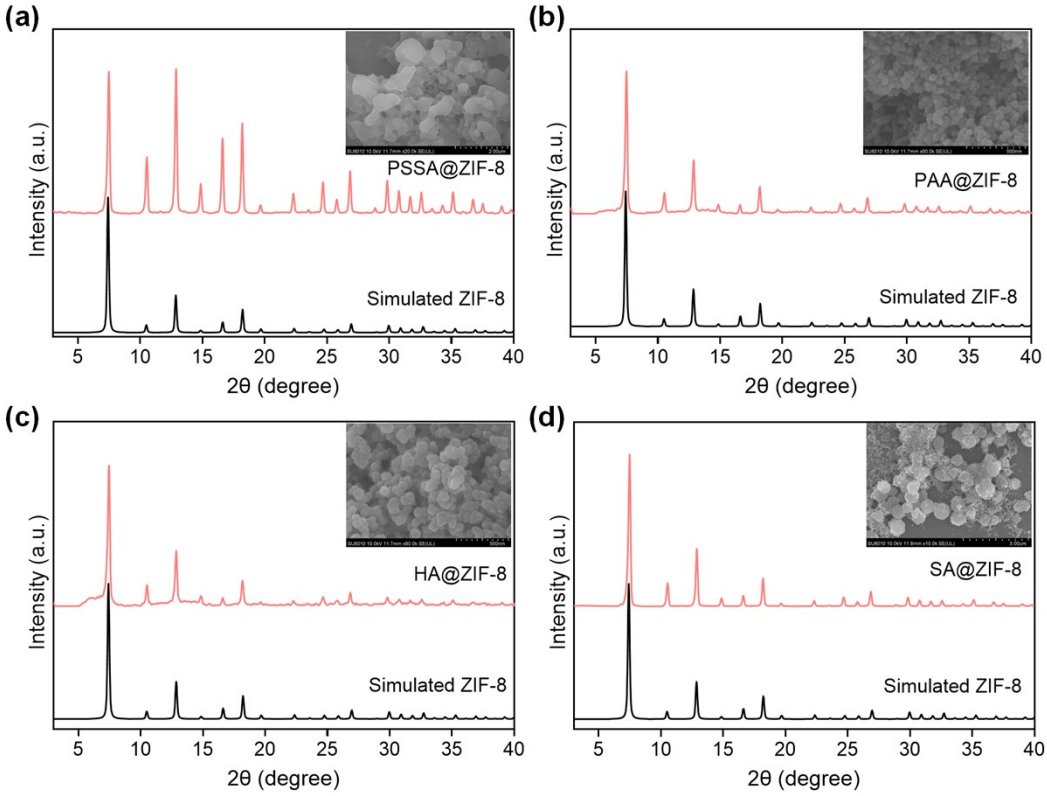

Fig. S4. PXRD pattern and SEM image of PSSA@ZIF-8, PAA@ZIF-8, HA@ZIF-8, and SA@ZIF-8 composites, evidencing the successful synthesis of ZIF-8 crystals.

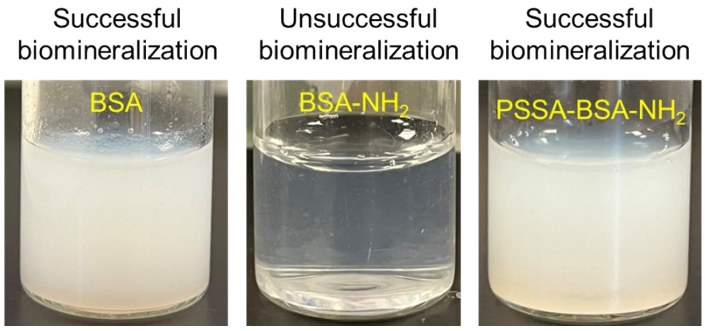

Fig. S5. The photographs recording the growth phenomenon of ZIF-8 minerals in the presence of BSA, BSA-NH_2, or PSSA-BSA-NH_2 complex. Conditions: BSA, BSA-NH_2 or PSSA-BSA-NH_2, 2 mg; Zn^{2+}, 40 mM; HmIM, 160 mM.

Note: The BSA and PSSA-BSA-NH_2 with negative surface charge could induce the ZIF-8 biomineralization to form BSA@ZIF-8 and PSSA-BSA-NH_2@ZIF-8 minerals, respectively, while the BSA-NH_2 with positive surface charge could not induce the ZIF-8 growth.

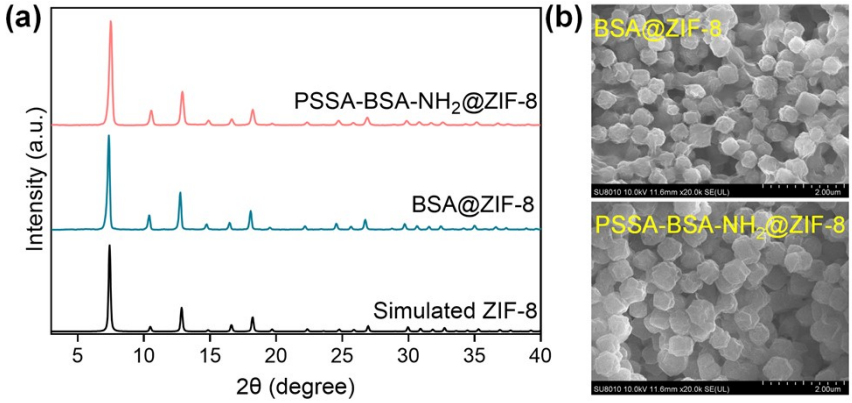

Fig. S6. PXRD patterns (a) and SEM images (b) of BSA@ZIF-8 and PSSA-BSA-NH_2@ZIF-8, evidencing the successful biosynthesis of ZIF-8 crystals.

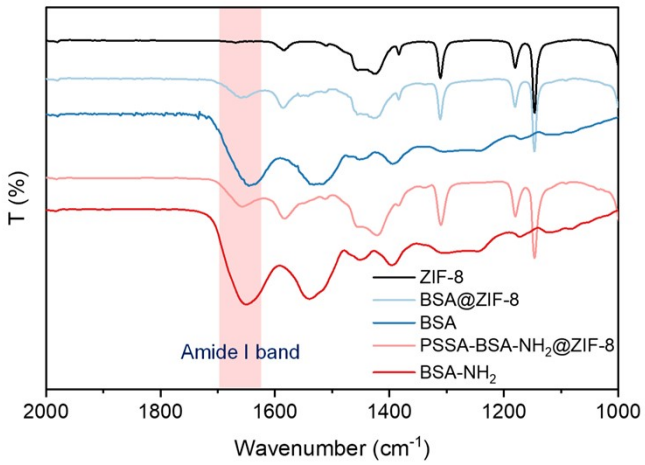

Fig. S7. FT-IR spectra of ZIF-8, BSA, BSA@ZIF-8, BSA-NH_2 and PSSA-BSA-NH_2@ZIF-8, demonstrating the existence of proteins within ZIF-8 biominerals.

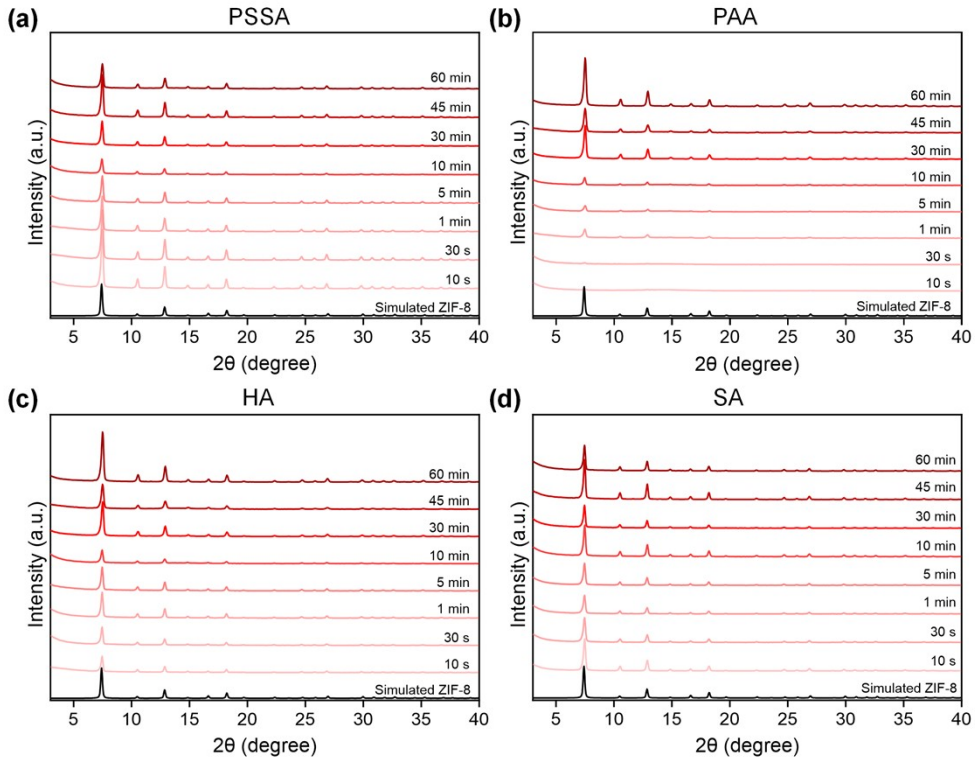

Fig. S8. PXRD patterns of PSSA-HRP@ZIF-8 (a), PAA-HRP@ZIF-8 (b), HA-HRP@ZIF-8 (c) and SA-HRP@ZIF-8 (d) biominerals aged for different time.

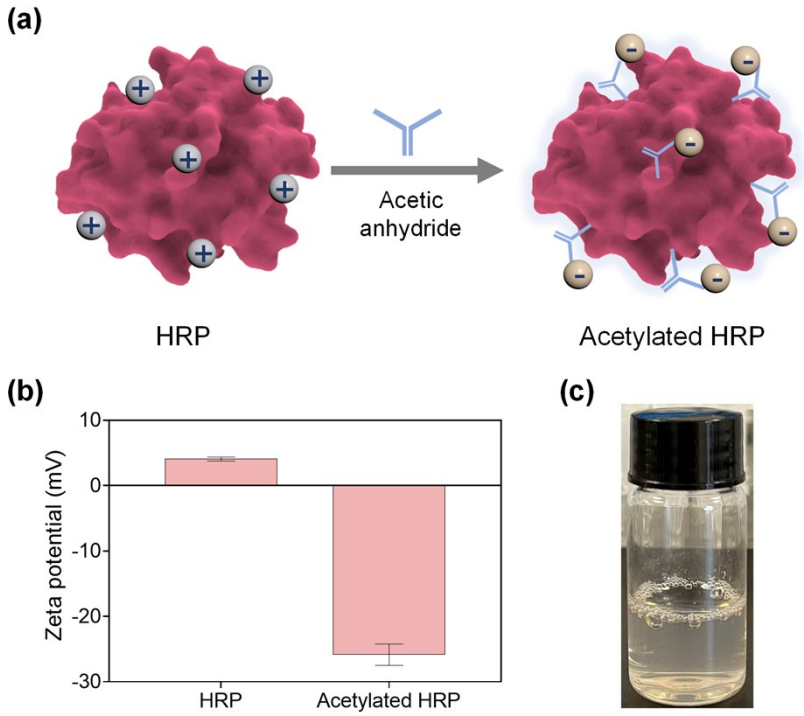

Fig. S9. (a) Schematic representation of altering the surface charge of HRP from positive to negative using acetic anhydride via a chemical coupling approach. (b) The zeta potential of HRP before and after acetylation. (c) The photographs recording the growth phenomenon of ZIF-8 minerals in the presence of acetylated HRP.

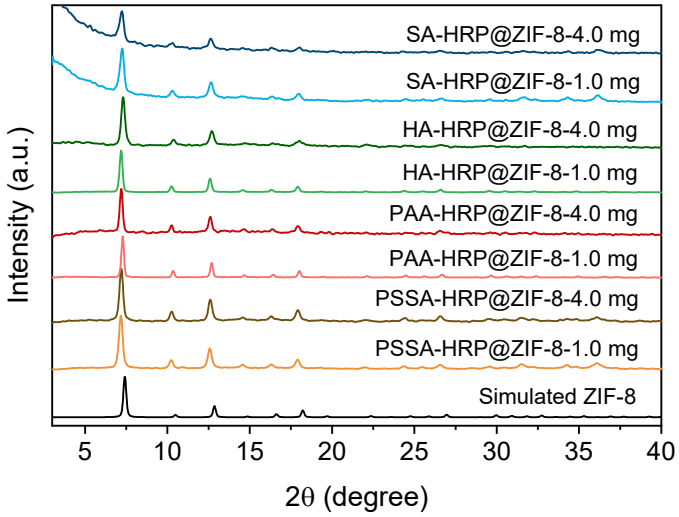

Fig. S10. PXRD patterns of the polymers-HRP@ZIF-8 biominerals synthesized by using 1.0 and 4.0 mg dosages of each polymer.

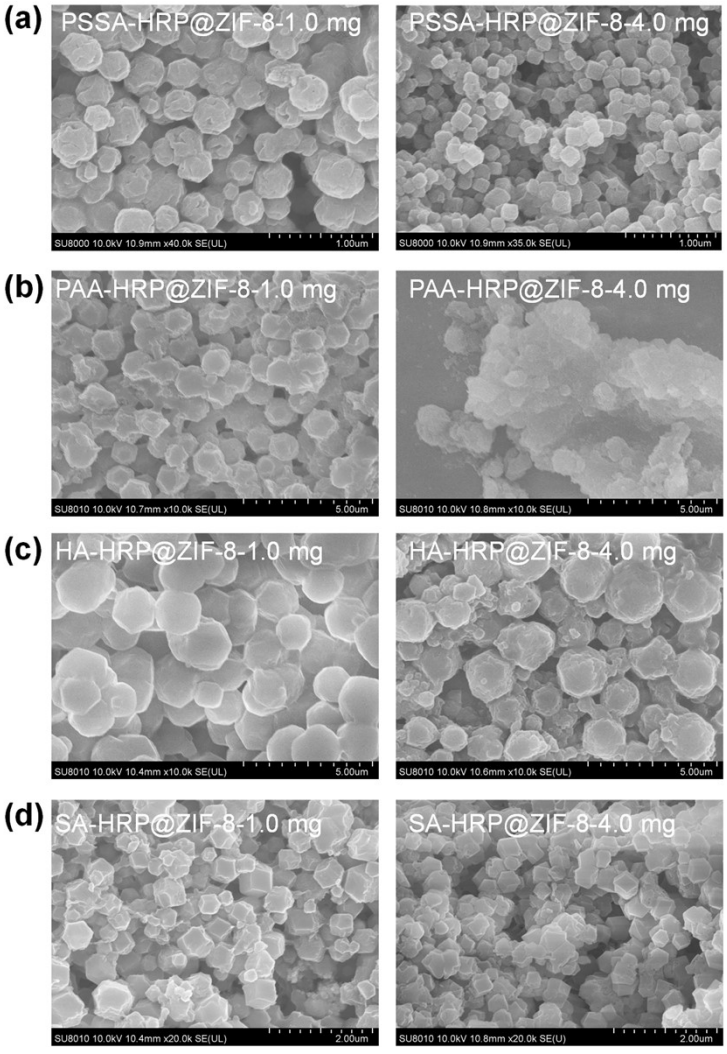

Fig. S11. SEM images of PSSA-HRP@ZIF-8 (a), PAA-HRP@ZIF-8 (b), HA-HRP@ZIF-8 (c), and SA-HRP@ZIF-8 (d) biominerals with different polymer dosages.

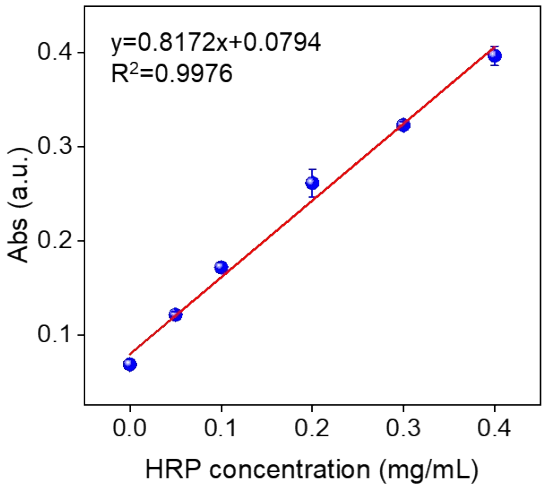

Fig. S12. Standard curve for the HRP quantification by a BCA method.

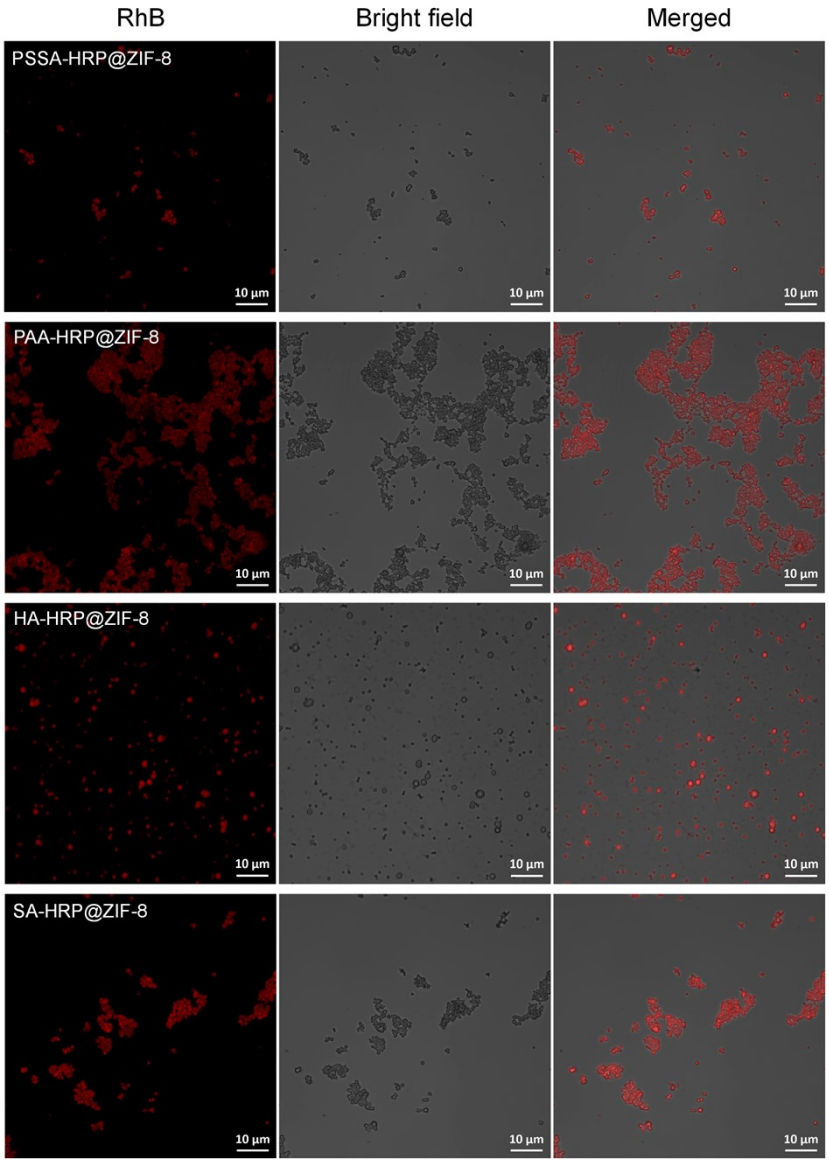

Fig. S13. The CLSM images of the polymers-HRP@ZIF-8 biominerals where the HRP was pre-labeled by RhB.

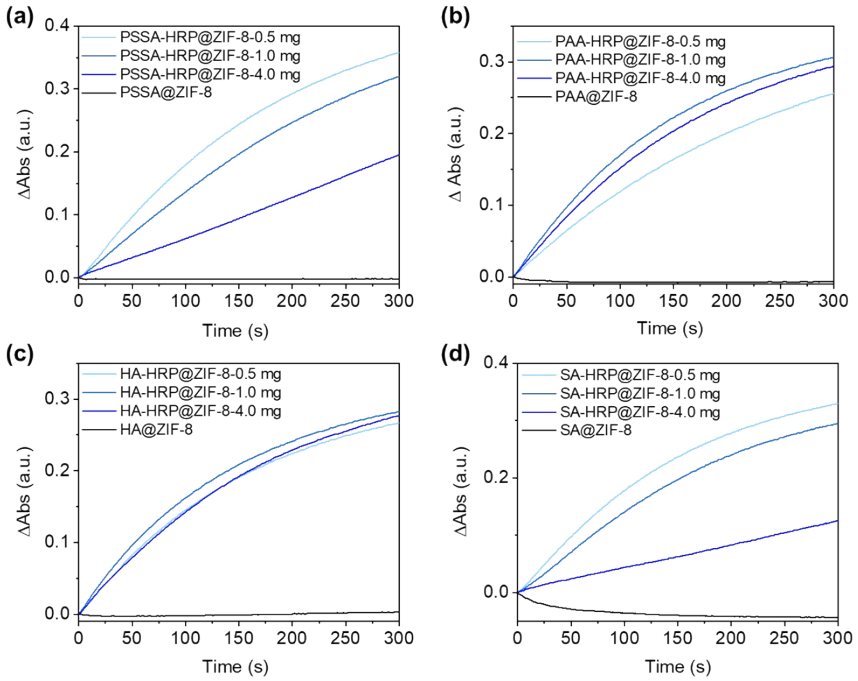

Fig. S14. Catalytic curves of the PSSA-HRP@ZIF-8 (a), PAA-HRP@ZIF-8 (b), HA-HRP@ZIF-8 (c), and SA-HRP@ZIF-8 (d) biominerals with different polymer dosages. The corresponding raw polymer induced ZIF-8 minerals including PSSA@ZIF-8, PAA@ZIF-8, HA@ZIF-8 and SA@ZIF-8 were used as negative controls.

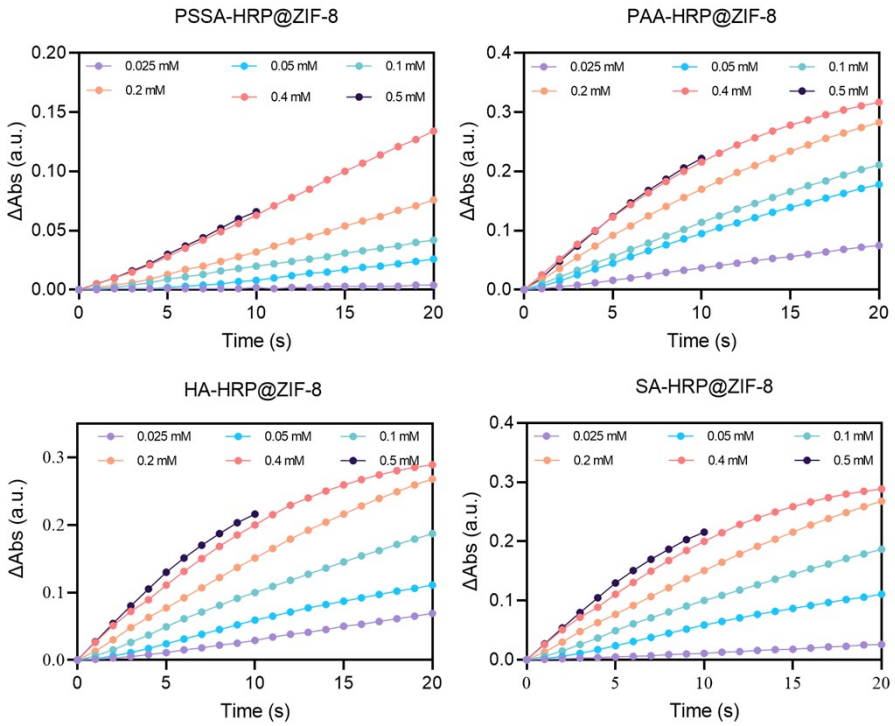

Fig. S15. The catalytic kinetic curves of PSSA-HRP@ZIF-8, PAA-HRP@ZIF-8, HA-HRP@ZIF-8 and SA-HRP@ZIF-8, respectively. HRP concentration was kept at 2.5 μg/mL.

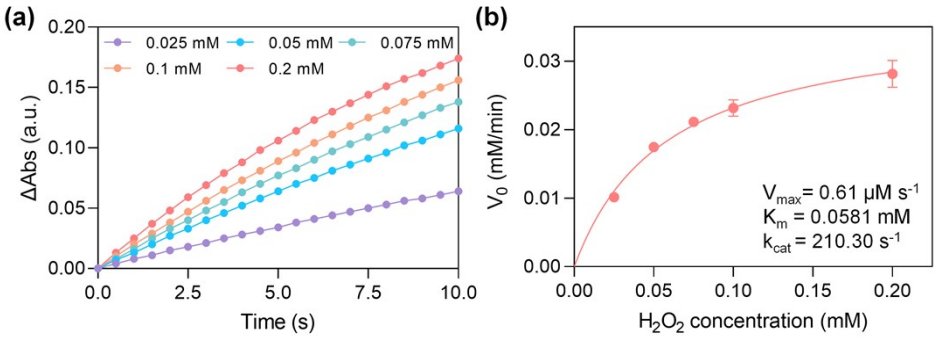

Fig. S16. (a) The catalytic kinetic curves of free HRP, in which the enzyme concentration was kept at 0.125 μg/mL. (b) The plot of initial catalytic rate (V_0) against substrate [H_2O_2] concentration for free HRP. Insets were the calculated kinetic parameters.

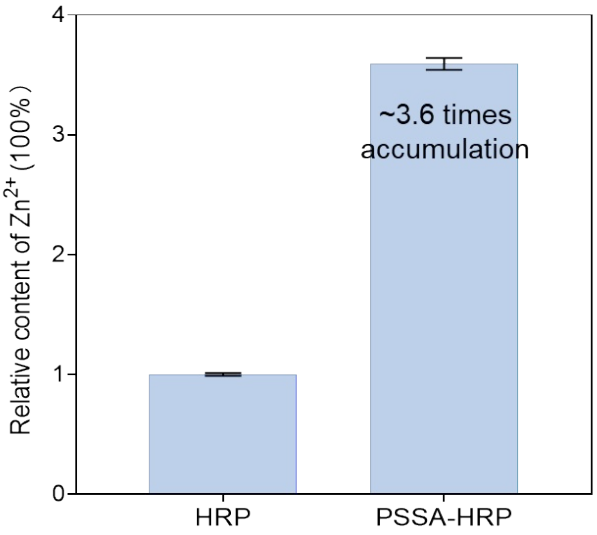

Fig. S17. Comparison of the accumulation contents of Zn^{2+} onto HRP before and after PSSA modification.

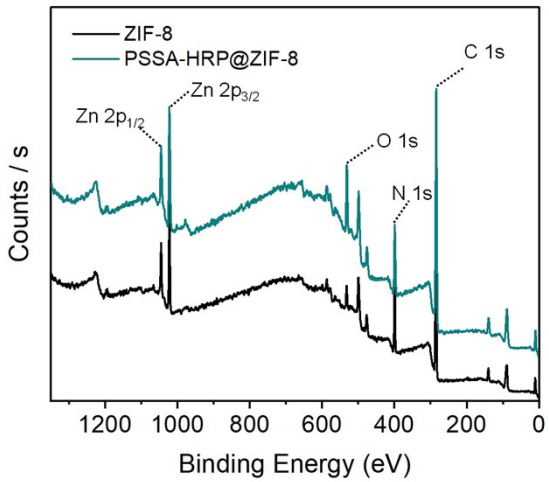

Fig. S18. XPS spectra of PSSA-HRP@ZIF-8 and pure ZIF-8.

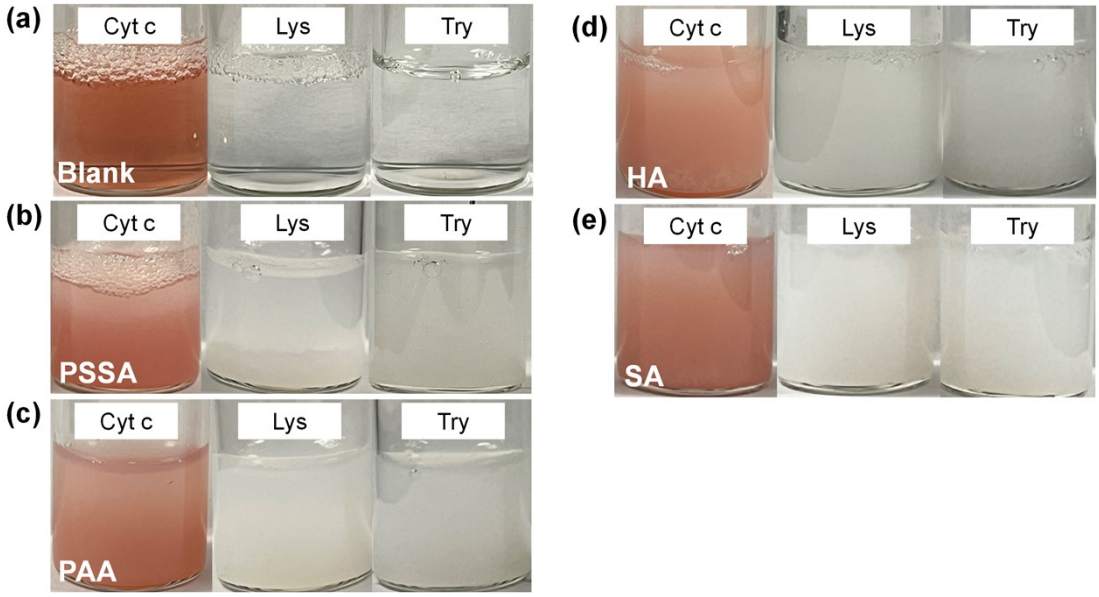

Fig. S19. Photographs recording the nucleation process. (a) The mixture of enzymes, HmIM and Zn^{2+} without polymer addition, and the solutions were transparent. (b-e) Precipitates were immediately produced when the Cyt c, Lys, and Try solutions were added with PSSA, PAA, HA and SA, respectively.

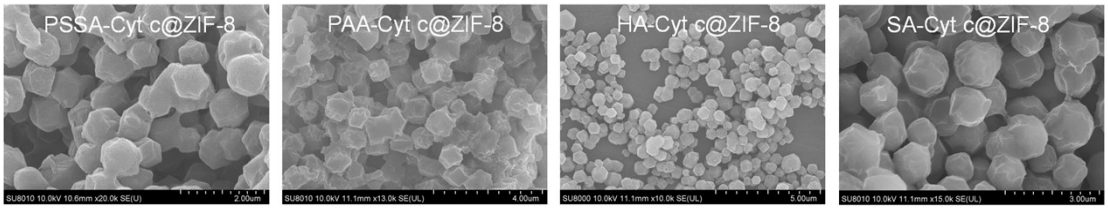

Fig. S20. SEM images of the polymers-Cyt c@ZIF-8 biominerals.

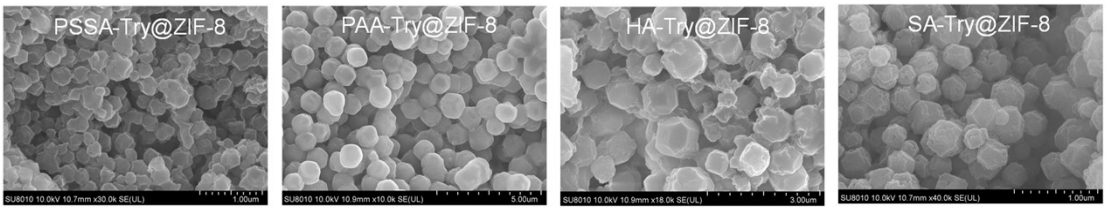

Fig. S21. SEM images of the polymers-Try@ZIF-8 biominerals.

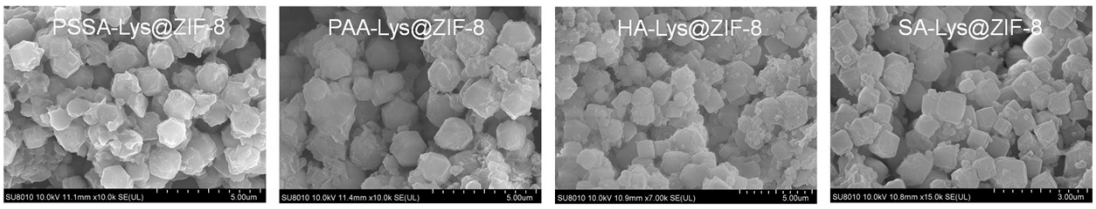

Fig. S22. SEM images of the polymers-Lys@ZIF-8 biominerals.

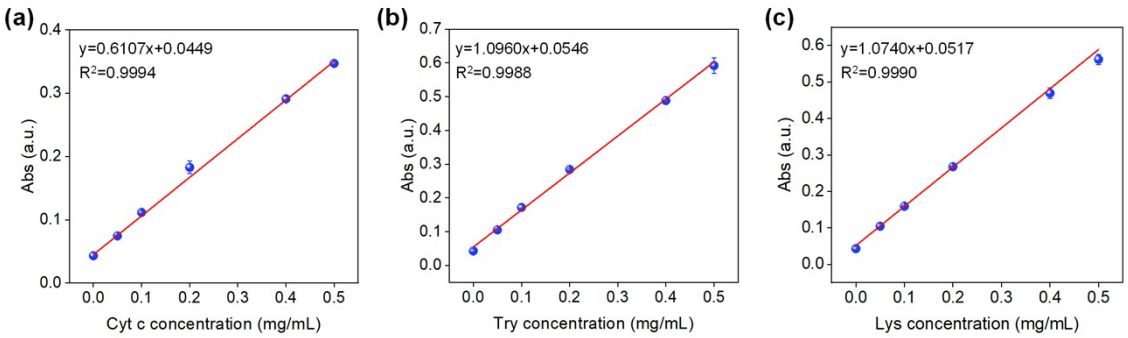

Fig. S23. The standard curves for the Cyt c, Try and Lys quantification using a BCA method.

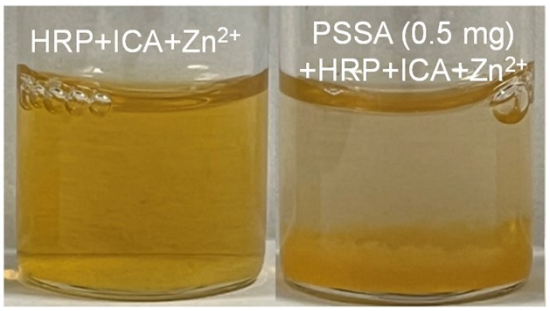

Fig. S24. Photographs recording the nucleation process of ZIF-90 on HRP in the absence and presence of PSSA.

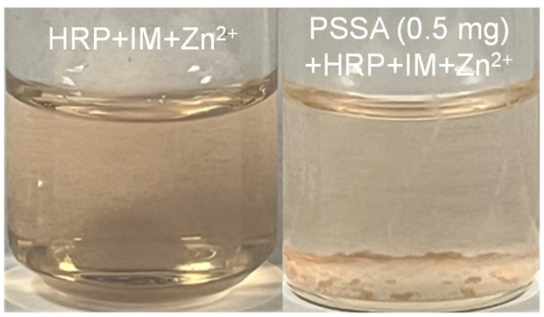

Fig. S25. Photographs recording the nucleation process of ZIF-zni on HRP in the absence and presence of PSSA.

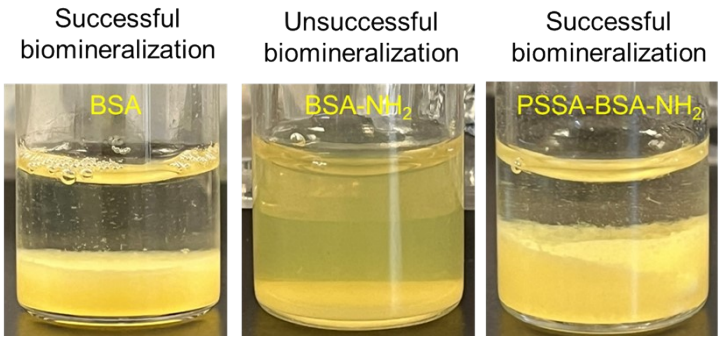

Fig. S26. The photographs recording the growth phenomenon of ZIF-90 minerals in the presence of BSA, BSA-NH_2 or PSSA-BSA-NH_2 complex. Conditions: BSA, BSA-NH_2 or PSSA-BSA-NH_2, 2 mg; Zn^{2+}, 40 mM; ICA, 160 mM.

Note: The BSA and PSSA-BSA-NH_2 with negative surface charge could also induce the ZIF-90 biomineralization to form BSA@ZIF-90 and PSSA-BSA-NH_2@ZIF-90 minerals, respectively, while the BSA-NH_2 with positive surface charge could not induce the ZIF-90 growth.

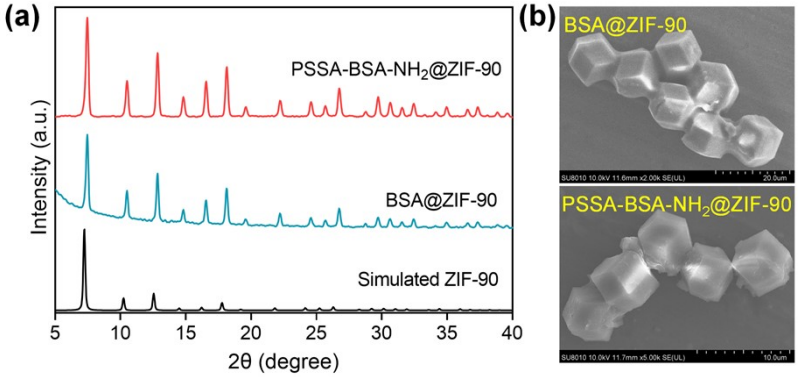

Fig. S27. PXRD patterns (a) and SEM images (b) of BSA@ZIF-90 and PSSA-BSA-NH_2@ZIF-90 biominerals, evidencing the successful biosynthesis of ZIF-90 crystals.

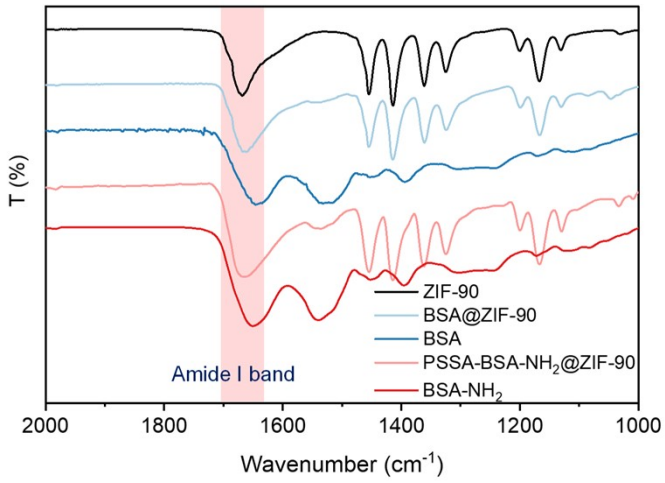

Fig. S28. FT-IR spectra of ZIF-90, BSA, BSA@ZIF-90, BSA-NH_2 and PSSA-BSA-NH_2@ZIF-90, demonstrating the presence of protein within the ZIF-90 biominerals.

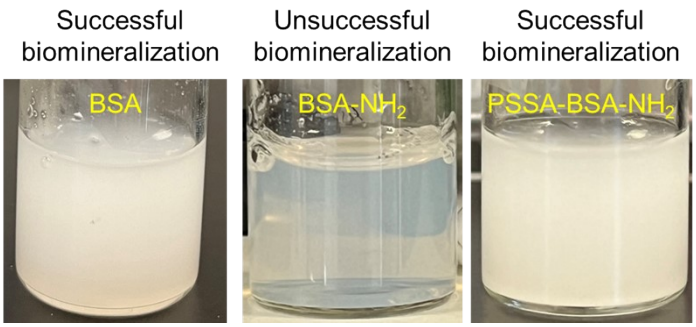

Fig. S29. The photographs recording the growth phenomenon of ZIF-zni minerals in the presence of BSA, BSA-NH_2 or PSSA-BSA-NH_2 complex. Conditions: BSA, BSA-NH_2 or PSSA-BSA-NH_2, 2 mg; Zn^{2+}, 40 mM; IM, 160 mM.

Note: The BSA and PSSA-BSA-NH_2 with negative surface charge could induce the ZIF-zni biomineralization to form BSA@ZIF-zni and PSSA-BSA-NH_2@ZIF-zni minerals, respectively, while the BSA-NH_2 with positive surface charge could not induce the ZIF-zni growth.

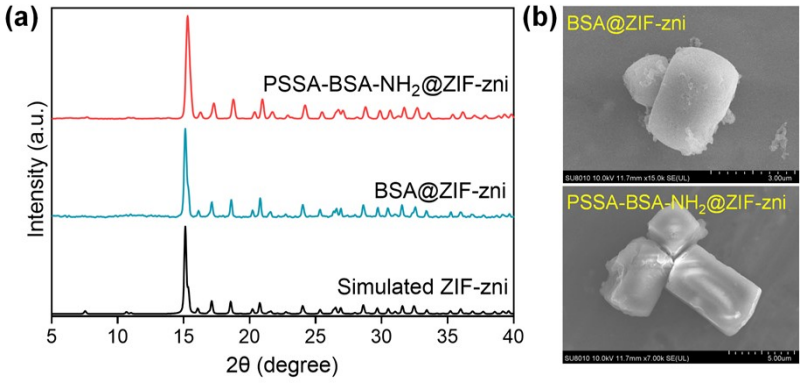

Fig. S30. PXRD patterns (a) and SEM images (b) of BSA@ZIF-zni and PSSA-BSA-NH_2@ZIF-zni biominerals, evidencing the successful biosynthesis of ZIF-zni crystals.

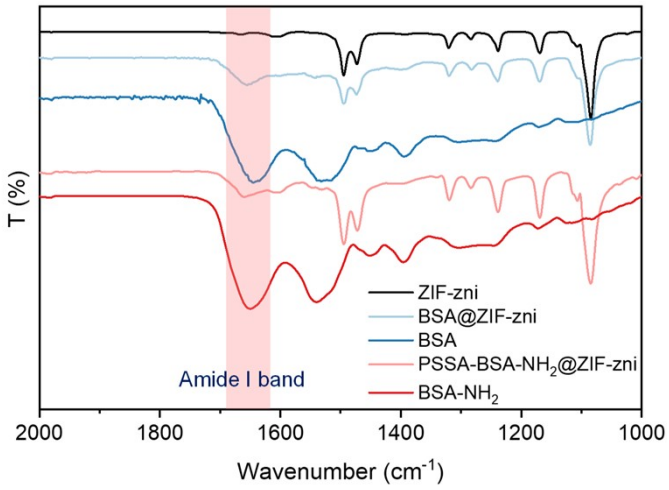

Fig. S31. FT-IR spectra of ZIF-zni, BSA, BSA@ZIF-zni, and PSSA-BSA-NH_2@ZIF-zni, demonstrating the presence of protein within the ZIF-zni biominerals.

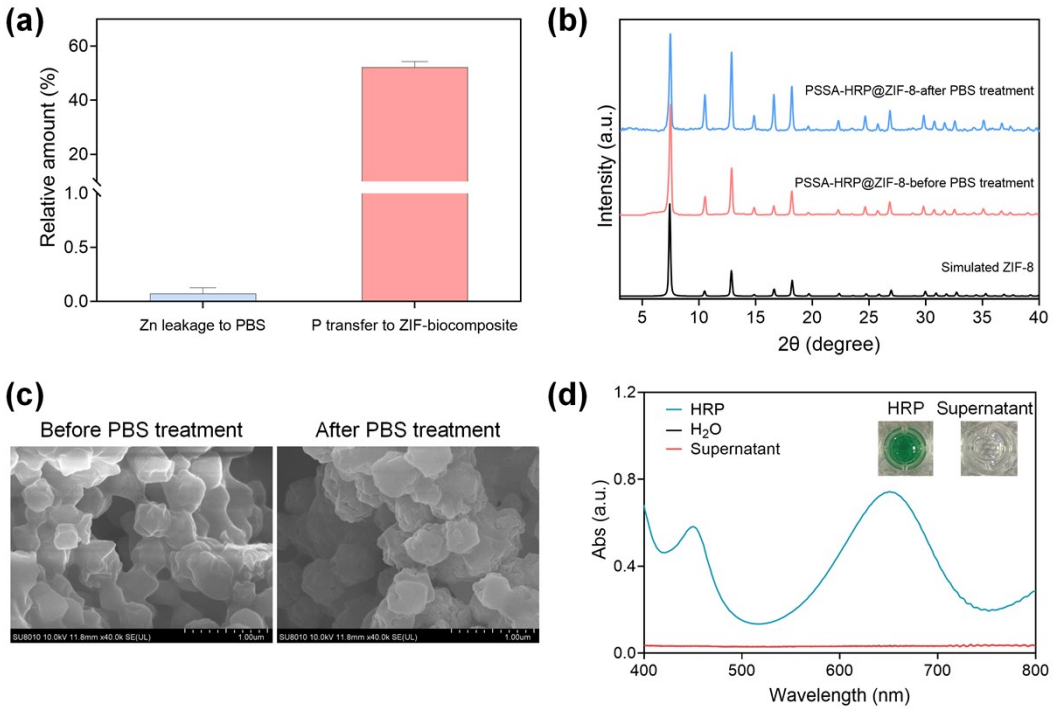

Fig. S32. (a) The relative amount of Zn content in the supernatant compared to that of the pristine PSSA-HRP@ZIF-8 biocomposite before 10 mM PBS treatment, and the relative amount of P content in the PBS-treated ZIF-biocomposite compared to that of the 10 mM PBS. (b,c) PXRD patterns (b) and SEM images (c) of PPSA-HRP@ZIF-8 before and after PBS treatment. (d) The UV-Vis spectra showing no catalytic activity of the PBS supernatant after treatment. HRP and H_2O were used as a positive and negative control, respectively.

Note: First, after the PSSA-HRP@ZIF-8 biocomposite was exposed to the PBS solution (10 mM) for 1 min, the leaked Zn content to the supernatant showed a proportion of 0.073% compared to the total Zn content in pristine biocomposte. Meanwhile, the remaining Zn content was almost the same as that of the pristine biocomposte (Table S6). The results indicated the negligible leakage of Zn^{2+} ions in the period of 1 min sensing. Nevertheless, the quantification results of P element displayed a 52.2% transfer from PBS solution to the ZIF-biocomposite, which might result from the P adsorption or coordination to the defective sites of ZIF-8. Besides, the SEM and PXRD pattern of the treated ZIF-biocomposite were maintained. The enzymatic activity measurement of the supernatant was not detected, indicating no HRP was leached out. Taking together, it was implied that during the rapid sensing assays, the biocomposite architecture was not yet decomposed and synchronously the HRP would be retained within the ZIF-8 biomineral.

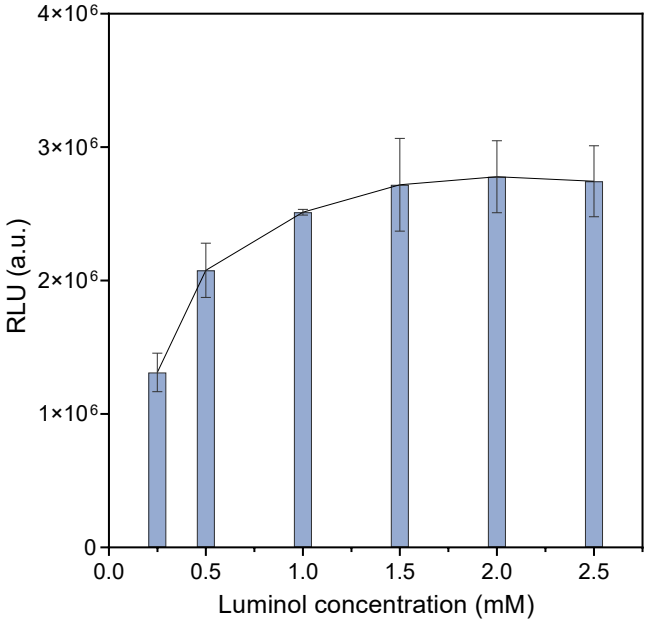

Fig. S33. The effect of luminol concentration on the chemiluminescence intensity.

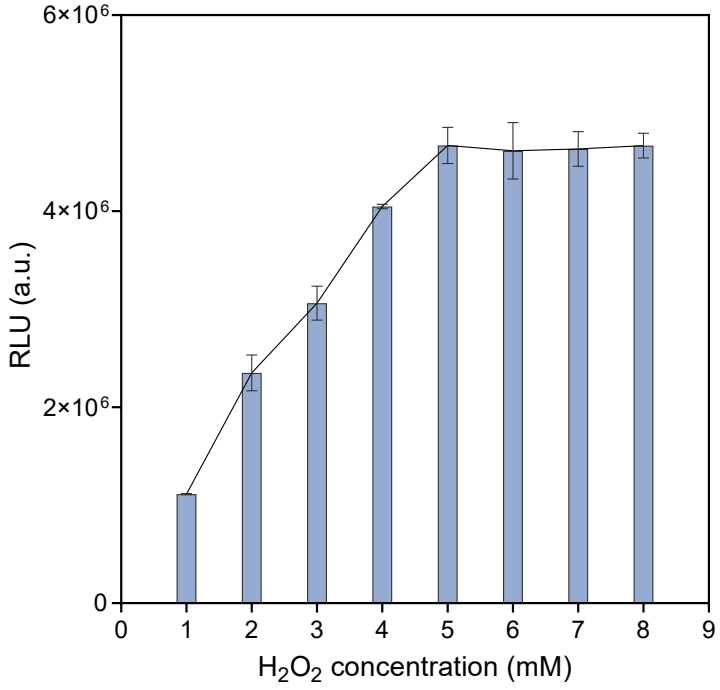

Fig. S34. The effect of H_2O_2 concentration on the chemiluminescence intensity.

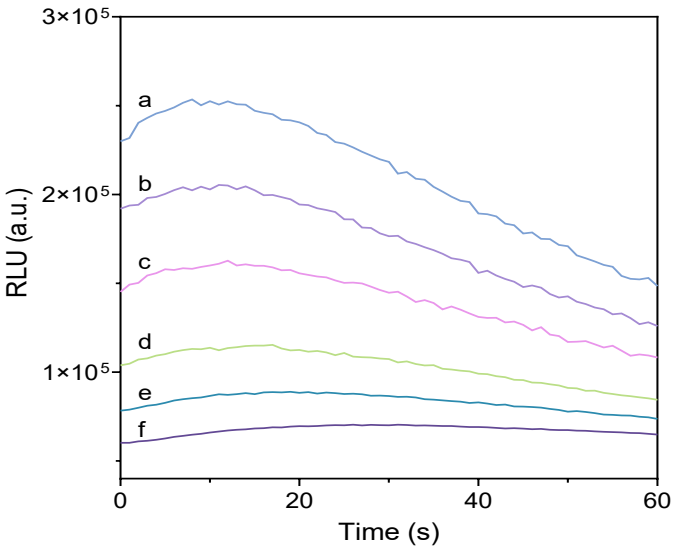

Fig. S35. Chemiluminescence response profiles of the developed biosensor under different concentrations of H_2S. Curves a to e represent 4.88, 9.77, 19.53, 39.06, 78.13 nM of H_2S, respectively, and curve f represents the baseline.

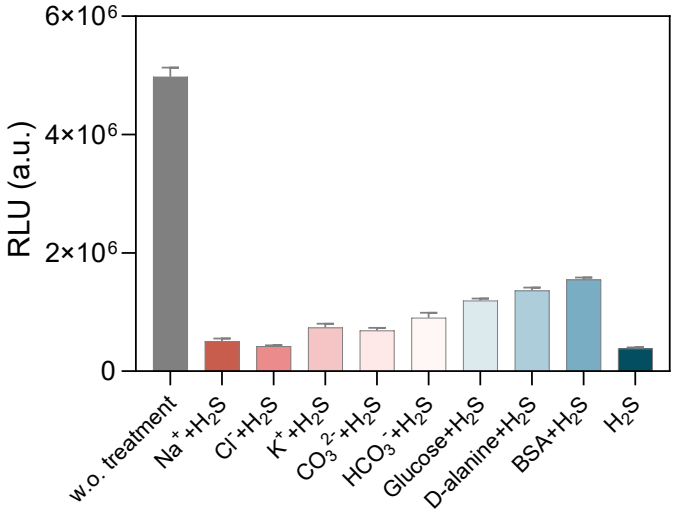

Fig. S36. The anti-interference experiments of the proposed H_2S biosensor. The concentrations of H_2S, BSA and the other interfering substances were 1 mM, 2 mM and 10 mM, respectively.

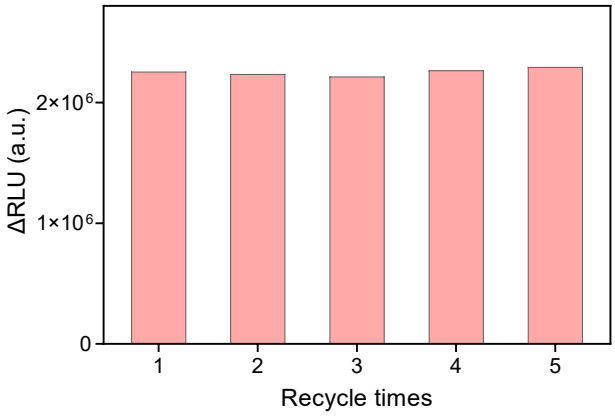

Fig. S37. Recyclability of the PSSA-HRP@ZIF-8 for H_2S sensing. The concentrations of HRP and H_2S in each cycle was kept at 0.1 mg/mL and 1 mM, respectively.

4. Supplementary References

[1] G. Chen, S. Huang, X. Kou, S. Wei, S. Huang, S. Jiang, J. Shen, F. Zhu and G. Ouyang, *Angew. Chem. Int. Ed.*, 2019, **58**, 1463-1467.

[2] K. Liang, R. Ricco, C. M. Doherty, M. J. Styles, S. Bell, N. Kirby, S. Mudie, D. Haylock, A. J. Hill, C. J. Doonan and P. Falcaro, *Nat. Commun.*, 2015, **6**, 7240.

[3] G. Chen, X. Kou, S. Huang, L. Tong, Y. Shen, W. Zhu, F. Zhu and G. Ouyang, *Angew. Chem. Int. Ed.*, 2020, **59**, 2867-2874.

[4] E. S. Bos, A. A. van der Doelen, N. van Rooy and A. H. Schuurs, *J. Immunoass. Immunoch.*, 1981, **2**, 187-204.

[5] D. Feng, T. Liu, J. Su, M. Bosch, Z. Wei, W. Wan, D. Yuan, Y. Chen, X. Wang, K. Wang, X. Lian, Z. Gu, J. Park, X. Zou and H. Zhou, *Nat. Commun.*, 2015, **6**, 5979.

[6] T. Lu and F. Chen, *J. Comput. Chem.*, 2012, **33**, 580-592.

[7] W. Humphrey, A. Dalke and K. Schulten, *J. Mol. Graph.*, 1996, **14**, 33-38.

[8] F. Chen, X. Xia, D. Ye, T. Li, X. Huang, C. Cai, C. Zhu, C. Lin, T. Deng and F. Liu, *Anal. Chem.*, 2023, **95**, 5773-5779.

[9] G. Chen, S. Huang, X. Kou, F. Zhu and G. Ouyang, *Angew. Chem. Int. Ed.*, 2020, **59**, 13947-13954.

[10] M. Zhao, Y. Li, X. Ma, M. Xia and Y. Zhang, *Talanta*, 2019, **200**, 293-299.

[11] K. Cheng, F. Svec, Y. Lv and T. Tan, *Small*, 2019, **15**, 1906245.

[12] X. Wu, J. Ge, C. Yang, M. Hou and Z. Liu, *Chem. Commun.*, 2015, **51**, 13408-13411.

[13] C. Hu, Y. Bai, M. Hou, Y. Wang, L. Wang, X. Cao, C. Chan, H. Sun, W. Li, J. Ge and K. Ren, *Sci. Adv.*, 2020, **6**, eaax5785.

[14] P. Sun, H. Chen, S. Lu, J. Hai, W. Guo, Y. Jing and B. Wang, *Anal. Chem.*, 2022, **94**, 11573-11581.

[15] S. Chen, J. Fan, M. Lv, C. Hua, G. Liang and S. Zhang, *Anal. Chem.*, 2022, **94**, 14675-14681.

[16] K. Yu, M. Li, H. Chai, Q. Liu, X. Hai, M. Tian, L. Qu, T. Xu, G. Zhang and X. Zhang, *Chem. Eng. J.*, 2023, **451**, 138321.

[17] L. Wu, Y. Ishigaki, Y. Hu, K. Sugimoto, W. Zeng, T. Harimoto, Y. Sun, J. He, T. Suzuki, X. Jiang, H. Chen and D. Ye, *Nat. Commun.*, 2020, **11**, 446.

[18] R. Wu, Z. Chen, H. Huo, L. Chen, L. Su, X. Zhang, Y. Wu, Z. Yao, S. Xiao, W. Du and J. Song, *Anal. Chem.*, 2022, **94**, 10797-10804.

[19] H. Ye, L. Sun, Z. Pang, X. Ji, Y. Jiao, X. Tu, H. Huang, X. Tang, Z. Xi and L. Yi, *Anal. Chem.*, 2022, **94**, 1733-1741.

[20] M. Mao, Y. Zu, Y. Zhang, Y. Qiu, Y. Lin, F. Luo, Z. Weng, C. Lin, B. Qiu and Z. Lin, *Anal. Chem.*, 2024, **96**, 4290-4298.

[21] J. Li, Y. Zhou, L. Song, S. Yang, Q. Wang, Y. Zhou, X. -B. Zhang, Z. Qing and R. Yang, *Anal. Chem.*, 2022, **94**, 15085-15092.

[22] J. Li, C. Zhu, W. Peng, X. Cao, H. Gao, M. Jiang, Z. Wu and C. Yu, *Anal. Chem.*, 2023, **95**, 2406-2412.

[23] Y. Geng, G. Zhang, Y. Chen, Y. Peng, X. Wang and Z. Wang, *Anal. Chem.*, 2022, **94**, 1813-1822.

[24] Z. Lu, J. Tan, Y. Wu, J. You, X. Xie, Z. Zhang, Z. Li and L. Chen, *Anal. Chem.*, 2023, **95**, 17089-17098.

[25] Q. Liu, Y. Liu, Q. Wan, Q. Lu, J. Liu, Y. Ren, J. Tang, Q. Su and Y. Luo, *Anal. Chem.*, 2023, **95**, 5920-5926.

[26] J. Zhu, Y. Xiao, W. Hu, Q. Cui, Y. Yuan, X. Peng, W. Wen, X. Zhang and S. Wang, *Anal. Chem.*, 2024, **96**, 1852-1860.

[27] L. Yan, Q. -S. Gu, W. -L. Jiang, M. Tan, Z. -K. Tan, G. -J. Mao, F. Xu and C. -Y. Li, *Anal. Chem.*, 2022, **94**, 5514-5520.

[28] J. Hou, Y. Huang, L. Fu, M. Sun, L. Wang, R. Guo, L. Chen and C. Lv, *Anal. Chem.*, 2023, **95**, 5514-5521.